Valley in the efficiency of the high-order harmonic yield at ultra-high laser intensities

J. A. Pérez-Hernández,[1,*] L. Roso,[1] A. Zaïr,[2] and L. Plaja[3]

[1]*Centro de Láseres Pulsados, CLPU, E-37008 Salamanca, Spain*
[2]*Department of Physics, Imperial College London, London, SW7 2AZ, UK*
[3]*Grupo de Investigación en Óptica Extrema (GIOE), Departamento de Física Aplicada, Universidad de Salamanca, Plaza de la Merced s/n, E-37008, Salamanca, Spain*

**joseap@usal.es*

Abstract: We study the process of high-order harmonic generation using laser pulses with non-adiabatic turn-on and intensities well above saturation. As a main point, we report the existence of a valley structure in the efficiency of single-atom high-order harmonic generation with increasing laser intensities. Consequently, after an initial decrease, the high-frequency radiation yield is shown to increase for higher intensities, returning to a level similar to the case below saturation. Such behavior contradicts the general belief of a progressive degradation of the harmonic emission at ultrahigh intensities, based on the experience with pulses with smoother turn-on. We shall show that this behavior corresponds to the emergence of a new pathway for high-order harmonic generation, which takes place during the pulse turn-on. Our study combines trajectory analysis, wavelet techniques and the numerical integration of 3-Dimensional Time Dependent Schrödinger Equation. The increase in efficiency raises the possibility of employing ultrahigh intensities to generate high-frequency radiation beyond the water window.

© 2011 Optical Society of America

OCIS codes: (020.2649) Strong field laser physics; (020.4180) Multiphoton processes; (190.2640) Harmonic generation and mixing; (190.4180) Multiphoton processes; (320.225) Femtosecond fenomena; (320.5540) Pulse shapping; (320.7110) Ultrafast non linear optics; (340.7480) X-rays, soft x-rays, extreme ultraviolet (EUV).

References and links

1. M. Ferray, A. L'Huillier, X. F. Li, L. A. Lompre, G. Mainfray, and C. Manus, "Multiple-harmonic conversion of 1064 nm radiation in rare gases," J. Phys. B, At. Mol. Opt. Phys. **21**, L31–L35 (1998).
2. J. L. Krause, K. J. Schafer, and K. C. Kulander, "High-order harmonic generation from atoms and ions in the high intensity regime," Phys. Rev. Lett. **68**, 3535–3538 (1992).
3. C. Spielmann, N. H. Burnett, S. Sartania, R. Koppitsch, M. Schnrer, C. Kan, M. Lenzner, P. Wobrauschek, and F. Krausz, "Generation of coherent X-rays in the water window using 5-femtosecond laser pulses," Science **278**, 661–664 (1997).
4. Z. Chang, A. Rundquist, H. Wang, M. M. Murnane, and H. C. Kapteyn, "Generation of coherent soft X rays at 2.7 nm using high harmonics," Phys. Rev. Lett. **79**, 2967–2970 (1997).
5. J. Seres, E. Seres, A. J. Verhoef, G. Tempea, C. Streli, P. Wobrauschek, V. Yakovlev, A. Scrinzi, C. Spielmann, and F. Krausz, "Laser technology: source of coherent kiloelectronvolt X-rays," Nature **433**, 596 (2005).
6. K. Schafer, B. Yang, L. F. DiMauro, and K. C. Kulander, "Above threshold ionization beyond the high harmonic cutoff," Phys. Rev. Lett. **70**, 1599–1602 (1993).

7. P. B. Corkum, "Plasma perspective on strong-field multiphoton ionization," Phys. Rev. Lett. **71**, 1994–1997 (1993).
8. J. Tate, T. Auguste, H. G. Muller, P. Salières, P. Agostini, and L. F. DiMauro, "Scaling of wave-packet dynamics in an intense midinfrared field," Phys. Rev. Lett. **98**, 013901 (2007).
9. J. A. Pérez-Hernández, L. Roso, and L. Plaja, "Harmonic generation beyond the strong-field approximation: the physics behind the short-wave-infrared scaling laws," Opt. Express **17**, 9891–9903 (2009).
10. J. A. Pérez-Hernández, J. Ramos, L. Roso and L. Plaja, "Harmonic generation beyond the strong-field approximation: phase and temporal description," Laser Phys. **20**, 1044–1050 (2010).
11. T. Popmintchev, M. C. Chen, O. Cohen, M. E. Grisham, J. J. Rocca, M. M. Murnane, and H. C. Kapteyn, "Extended phase matching of high harmonics driven by mid-infrared light," Opt. Lett. **33**, 2128–2130 (2008).
12. P. Moreno, L. Plaja, V. Malyshev, and L. Roso, "Influence of barrier suppression in high-order harmonic generation," Phys. Rev. A **51**, 4746–4753 (1995).
13. V. V. Strelkov, A. F. Sterjantov, N. Yu Shubin, and V. T. Platonenko, "XUV generation with several-cycle laser pulse in barrier-suppression regime," J. Phys. B, At. Mol. Opt. Phys. **39**, 577-589 (2006).
14. H. Xiong, H. Xu, Y. Fu, J. Yao, B. Zeng, W. Chu, Y. Cheng, Z. Xu, E. J. Takahashi, K. Midorikawa, and X. Liu, and J. Chen, "Generation of a coherent x ray in the water window region at 1 kHz repetition rate using a mid-infrared pump source," Opt. Lett. **34**, 1747–1749 (2009).
15. P. Arpin, T. Popmintchev, N. L. Wagner, A. L. Lytle, O. Cohen, H. C. Kapteyn, and M. M. Murnane, "Enhanced high harmonic generation from multiply ionized argon above 500 eV through laser pulse self-compression," Phy. Rev. Lett. **103**, 143901 (2009).
16. F. Ferrari, F. Calegari, M. Lucchini, C. Vozzi, S. Stagira, G. Sansone, and M. Nisoli, "High-energy isolated attosecond pulses generated by above-saturation few-cycle fields," Nat. Photonics **4**, 875–879 (2010).
17. K. T. Kim, C. M. Kim, M. G. Baik, G. Umesh, and C. H. Nam, "Single sub-50-attosecond pulse generation from chirp-compensated harmonic radiation using material dispersion," Phys. Rev. A **69**, 051805 (2004).
18. T. Sekikawa, A. Kosuge, T. Kanai, and S. Watanabe, "Nonlinear optics in the extreme ultraviolet," Nature **432**, 605–608 (2004).
19. M. Schnürer, Ch. Spielmann, P. Wobrauschek, C. Streli, N. H. Burnett, C. Kan, K. Ferencz, R. Koppitsch, Z. Cheng, T. Brabec, and F. Krausz, "Coherent 0.5-keV X-ray emission from helium driven by a sub-10-fs laser," Phys. Rev. Lett. **80**, 3236–3239 (1998).
20. M. Geissler, G. Tempea, and T. Brabec, "Phase-matched high-order harmonic generation in the nonadiabatic limit," Phys. Rev. A **62**, 033817 (2000).
21. J. Wu, H. Cai, A. Couairon, and H. Zeng, "Few-cycle shock X-wave generation by filamentation in prealigned molecules," Phys. Rev. A **80**, 013828 (2009).
22. J. Wu, H. Cai, Y. Peng, and H. Zeng, "Controllable supercontinuum generation by the quantum wake of molecular alignment," Phys. Rev. A **79**, 041404 (2009).
23. H. Cai, J. Wu, Y. Peng, and H. Zeng, "Comparison study of supercontinuum generationby molecular alignment of N_2 and O_2," Opt. Express **17**, 5822–5828 (2009).
24. H. Cai, J. Wu, X. Bai, H. Pan, and H Zeng, "Molecular-alignment-assisted high-energy supercontinuum pulse generation in air," Opt. Lett. **35**, 49–51 (2010).
25. J. Vazquez de Aldana and L. Roso, "Magnetic-field effect in atomic ionization by intense laser fields," Opt. Express **5**, 144–148 (1999).

1. Introduction

In strong field interactions, high order non-linear processes appear with efficiencies much higher than those expected by conventional perturbative approaches. In particular, the harmonic emission spectrum is characterized by the emergence of a plateau structure in which, for several orders, the intensity of the harmonics remains at similar levels [1]. For atomic and molecular gaseous targets, the harmonic plateau cut-off frequency is given by $\hbar\omega_c \simeq I_p + 3.17U_p$ [2], where I_p is the ionization potential, and U_p is the electron ponderomotive energy $U_p \propto I\lambda^2$ (I being the laser intensity and λ the wavelength). For the usual high-power laser wavelengths ($\simeq 800nm$) the spectral plateau extends to the XUV region, and beyond the water window [3–5], providing sources for high-frequency coherent radiation potentially useful for biological imaging and applications.

In the intense field regime, high-order harmonics are generated by ionized electrons [6, 7]. Once in the continuum, the electrons are accelerated by the field and driven back to scatter with the parent ion. During the recollision, the overlap between the continuum and bound state wavefunctions gives rise to a fast oscillating dipole and, therefore, to the generation of radi-

ation. The spectral cut-off is, then, explained by the maximum kinetic energy of the ionized electron upon recollision ($3.17U_p$). Consequently, the emission of higher frequencies requires either increasing the wavelength or increasing intensity of the driving laser. However, these two strategies are not equivalent as they affect differently the ionization process. On one hand, increasing the wavelength approaches the ideal tunnel ionization with static fields. Even though there is no fundamental limitation in this method, the harmonic yield is shown to decrease strongly with wavelength [8–10]. Nevertheless, this loss in efficiency can be compensated by optimizing the phase matching conditions at the target [11]. On the other hand, reaching shorter wavelengths by the increase of intensity is known to be limited by the saturation of ionization. Above this threshold the harmonic yield is known to decrease [12, 13], and also the generated plasma affects negatively the phase matching of the harmonic propagation. These limitations seem fundamental and discourages adopting this second strategy for the generation of shorter wavelengths [14]. Note, however, that as the neutral atom is depleted, ions can become alternative sources of ultra-high order harmonic generation as demonstrated experimentally in [15]. There are potential advantages for considering ultrahigh intensities as a method to extend the harmonic plateau. For example this approach does not require the development of new intense sources, as the current technology of Ti:Sa amplifiers provides already ultrashort pulses with intensities well above saturation of commonly used targets. Additionally, ultrashort pulses with intensities above threshold are demonstrated to produce phase-locked structureless spectra, permitting the generation of isolated XUV pulses with durations below 50 attoseconds [16–19].

For the particular case of pulses leading to complete depletion of the ground state in less than an optical cycle (referred here as Non-Adiabatic Turn-on, NAT), the harmonic propagation is shown to be benefited by the non-adiabatic self-phase-matching [20]. More recently, the robustness of the single-atom results against propagation for NAT pulses has been also confirmed numerically [16]. In light of these results, the main limitation for using ultrahigh intensities to generate shorter wavelengths would be the degradation of the harmonic yield with intensity in the single-atom response. The aim of this paper is to demonstrate that this degradation can be avoided using NAT pulses. In particular, we shall show in the single atom response that it is possible to generate high-frequency radiation using intensities about two orders of magnitude above the saturation threshold. At such intensities, the extension of the spectrum reaches short wavelengths in the soft X-Ray region ($\leq 1nm$), reaching the present frontier of high-order harmonic generation [5]. We should stress that the ultrahigh intensities considered here are one order of magnitude above those in [16], where the decrease of the harmonic yield was not yet observable. We should note that the possibility of generating pulses with rapid rising edges has been recently reported in the context of filamentation in molecular aligned gases [21–24]

2. Theoretical Approach

2.1. Trajectory Analysis

The fundamental aspects of high-order harmonic generation can be retrieved studying the trajectories of electrons [6, 7]. After ionization, the electron is assumed as a classical free particle located at the ion's coordinate, with zero velocity. The particle's trajectory can be then computed by integrating the Newton-Lorentz equation in the dipole approximation. The first crossing of the electron's trajectory with the ion coordinate describes the first rescattering, when the electron's kinetic energy is released in the form of radiation. Figure 1(a) plots the rescattering kinetic energy as a function of the ionization time (blue curve) and as a function of the rescattering time (black curve) for a field with constant envelope. The most energetic trajectories correspond to electrons ionized near the field maxima, that recollide with the ion at approximately 3/4 of a cycle later. In the following, we will refer to these as SC trajectories, as they were proposed by Schafer *et al* [6] and Corkum [7] to explain the plateau's cut-off law. The

two first sets of SC trajectories are labelled SC-long and SC-short in Fig. 1. Part b of the figure shows the same trajectory analysis for a NAT pulse. In this particular case, we have chosen an ultrashort pulse (1.5 cycles FWHM) with the explicit form

$$E(t) = E_0 \sin^2\left(\frac{\omega t}{6}\right)\sin(\omega t + \phi) \tag{1}$$

where E_0 is the field amplitude, and ϕ is the carrier-envelope phase (in the following $\phi = 0$, unless otherwise is specified).

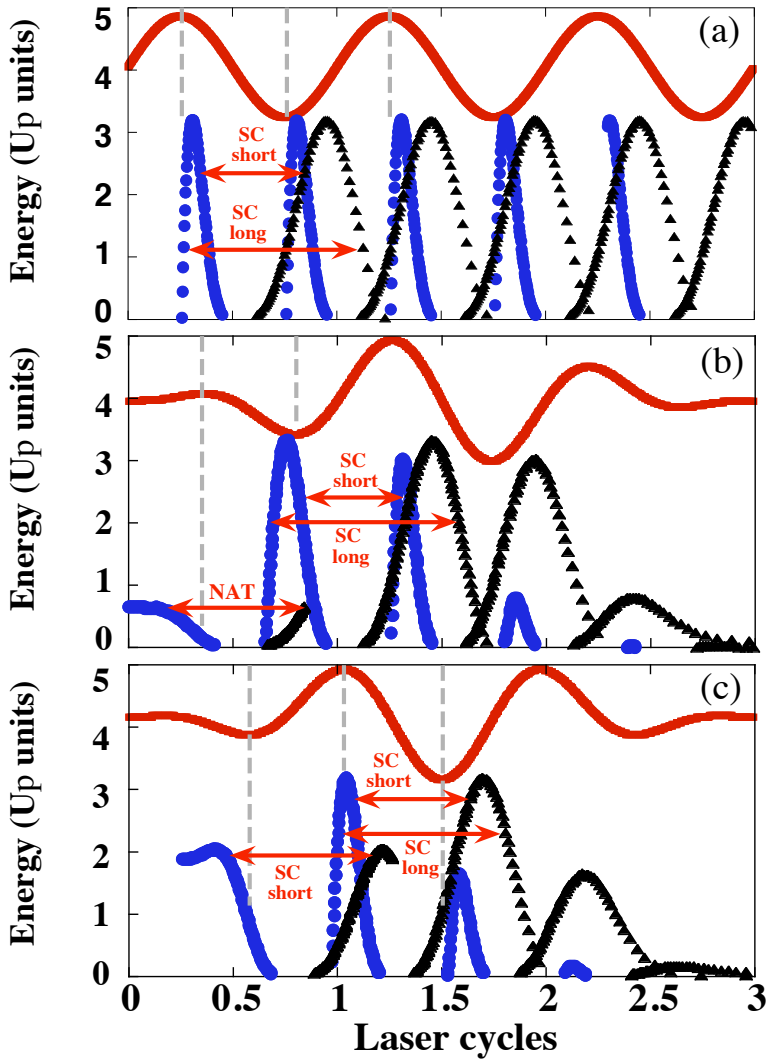

Fig. 1. Rescattering energies of electrons as a function of the ionization time (blue circles) and recollision time (black triangles), for laser pulses of (a) constant envelop, and (b) and (c) as described in Eq. (1) with (b) $\phi = 0$ and (c) $\phi = \pi/2$. A sketch of the driving field used in each case is shown as solid red lines. Note that for the case $\phi = 0$, appears the special set of trajectories in the turn-on of the pulse, labeled as NAT.

Through the analysis of Fig. 1(b) it is possible to identify two different classes of trajectories.

The first class of trajectories is characterized by electrons ionized at the last part of the turn-on and later follow trajectories with similar characteristics as the SC type, i.e. with the most energetic recollisions corresponding to electrons ionized near the field maxima. The second class of trajectories labeled as NAT correspond to the electrons ionized during the initial part of the turn on. These follow the opposite trend: the most energetic rescatterings originate from electrons ionized almost a quarter cycle before the first field maximum. The emergence of these trajectories is connected with the fast turn-on of the laser pulse, therefore we will refer them as NAT trajectories.

As mentioned above, for pulses with adiabatic turn-on, the harmonic yield is degraded when generated with laser intensities above saturation [12, 13]. Next, we shall see that this is connected to the decay in efficiency of the radiation generated by SC type trajectories. As discussed in the following, this decay is due to the fast ionization of the ground state during the excursion of the electron through the continuum. As a result, at the time of rescattering, the ground state is depopulated and the dipole amplitude is small and it results in a lack of efficiency in the HHG produced by SC types trajectories. We will also demonstrate that NAT trajectories are particularly resistant to the effects of saturation and, therefore, play the fundamental role in harmonic generation with ultraintense fields.

An evaluation of the relative contributions to the harmonic spectrum of the different trajectories can be drawn by estimating the absolute value of the complex dipole amplitude (assuming constant transition matrix elements)

$$|d(t)| \propto |a_0^*(t)||a_{\mathbf{v}}(t)| \tag{2}$$

where $a_0(t)$ is the probability amplitude of the ground state and $a_{\mathbf{v}}(t)$ is the probability amplitude of the free electron state with velocity v, at the time of rescattering t. The values for the probability amplitudes are extracted from the results of the exact 3D numerical integration of the time-dependent Schrödinger equation (TDSE): $|a_0(t)|$ is found projecting of the total wavefunction on the ground state, and $|a_v(t)|$ is estimated computing the ground-state depletion during a small time-window around the corresponding ionization time t_0 (i.e. the initial time of the trajectory associated to the rescattering at time t). Specifically

$$|a_v(t)|^2 \simeq \frac{d}{dt}|a_0|^2\bigg|_{t_0} \Delta t \tag{3}$$

with Δt being a small time interval, whose particular value is not important for the relative comparison between different trajectories, as long as it is kept unchanged. The values of the ionization and rescattering times (t_0 and t) for a particular trajectory are extracted from the classical analysis of Fig. 1. This permits us to associate each pair (t_0, t) to a well-defined trajectory of the NAT or SC type. In order to compare the harmonic efficiency at different laser intensities, we focus on the yield at a fixed energy, W_0.

Then, for each laser intensity, we use Fig. 1 to determine the ionization time t_0, and the rescattering time t corresponding to the electronic trajectories with recollision kinetic energy $W_0 - I_p$. We use W_0=73 eV, corresponding to the cut-off energy of the harmonic spectrum in hydrogen at the threshold intensity for saturation [13] (see Fig. 3). The results for the estimations of the harmonic efficiencies at W_0 using different laser intensities are shown in Fig. 2(a), for the short pulse considered in Fig. 1(b). SC curves in Fig. 2(a) show a descendent behavior with increasing field amplitude, which is connected with the degradation of the harmonic generation by these type of trajectories . The reason behind this can be found in the analysis of the probability amplitudes that conform the dipole transition, as written in Eq. (2). Figure 2(b) and Fig. 2(c) show the probability amplitudes of the ground and continuum states at rescattering, $|a_0(t)|$ and $|a_v(t)|$. As it is apparent, the decrease in the efficiency of the harmonics radiated by SC type

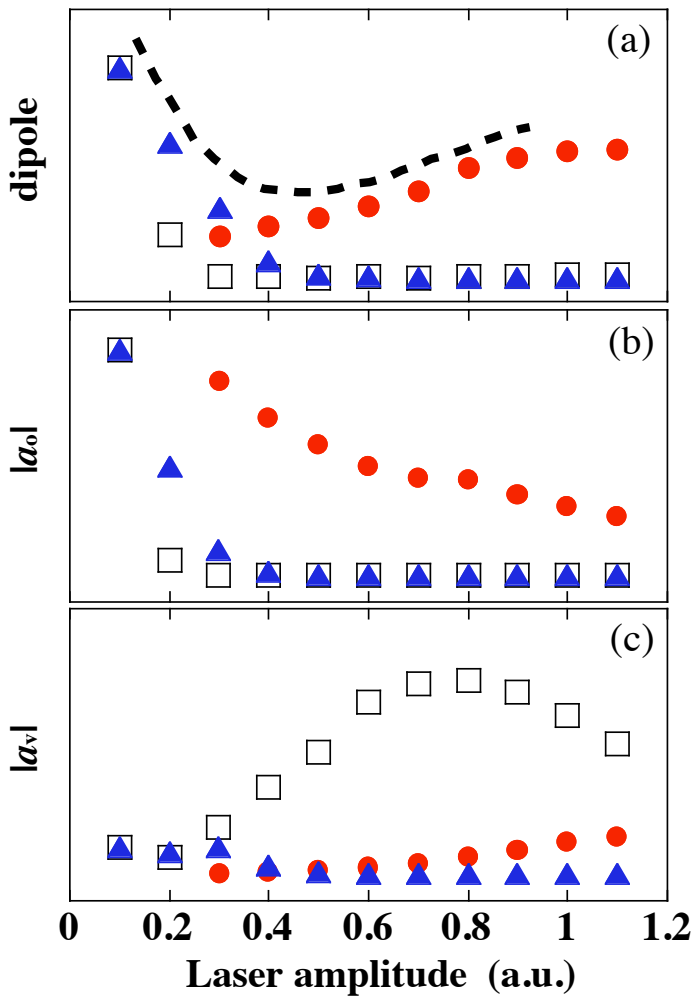

Fig. 2. Estimations of (a) the relative contributions to the harmonic yield at $W_0 = 73$ eV, (b) the probability amplitude of the ground state, and (c) the corresponding continuum state at the moment of recollision for the sets of trajectories highlighted in Fig. 1(b). Contributions of NAT trajectories are shown as red circles, long SC trajectories as open squares and short SC as blue triangles. The dashed line in (a) is a sketch of the resulting valley structure for the total radiation yield (sum of the above contributions). The laser amplitudes E are given in atomic units, corresponding to intensities $E^2 \times 3.5 \times 10^{16} W/cm^2$.

trajectories is connected with the fast ionization of the ground state for intensities above saturation and, therefore, with the decrease of $|a_0|$. Despite the fact that depletion of the ground state population increases the population of electrons in the continuum, i.e. $|a_{\mathbf{v}}|$ increases when $|a_{\mathbf{0}}|$ decreases, the product of both amplitudes has a net decrease and the efficiency of the dipole transition falls. In contrast, for the case of NAT trajectories, the behavior is the opposite: as they are originated at the first part of the turn-on, the ionization is moderate, even in the case of field amplitudes one order of magnitude above saturation (i.e. intensities two orders of magnitude above saturation). At rescattering, therefore, there is still a significant population in the ground state, and the product of probability amplitudes does not vanish. Therefore, the dipole ampli-

tude is found to increase gradually with the field amplitude. As a result, the global behavior of the harmonic yield with the laser amplitude (Fig. 2(a)) follows the form of a valley: First, a decrease connected with the degradation of the efficiency of the SC trajectories, followed by an increase as the efficiency of the NAT trajectories becomes the relevant contribution to the dipole spectrum. NAT trajectories will eventually be degraded for ultraintense fields well above the atomic unit ($3.51 \times 10^{16}\ W/cm^2$), however for these intensities we should expect also a decay connected with the breaking of the dipole approximation and the associated drift of the electron trajectories away from the ion due to the interaction with the magnetic field [25].

2.2. Harmonic Spectrum and Synthesis of Attosecond Pulses

In order to test our analysis, Fig. 3 shows the spectra at intensities corresponding to threshold of saturation, saturation and deep saturation regimes, extracted from the exact integration of the 3D TDSE in Hydrogen. Below and at the saturation threshold ($I \leq 3.51 \times 10^{14}$ W/cm^2) the increase in laser intensity does not affect strongly the harmonic yield, although it extends the harmonic plateau accordingly to the cut-off law mentioned before. Above saturation the harmonic yield begins to decrease until a minimum is reached at $I \simeq 5.6 \times 10^{15}$ W/cm^2, corresponding to the bottom of the valley structure sketched in Fig. 2(a). For higher intensities the harmonic yield increases as a consequence of the emergence of the contribution of the NAT-type trajectories to the radiation spectrum.

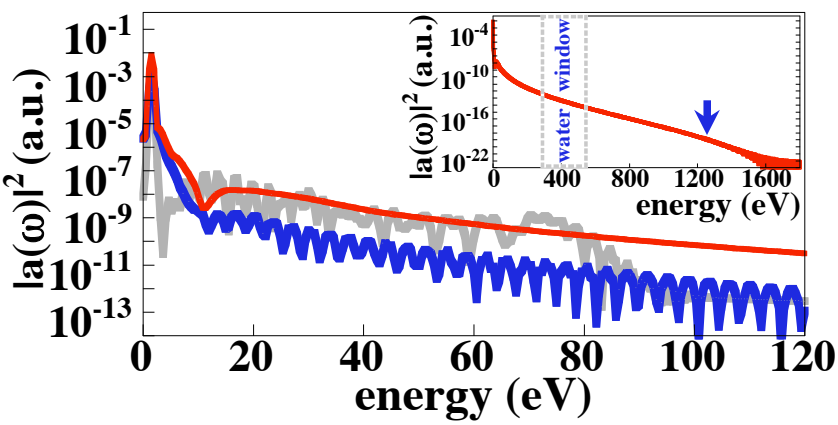

Fig. 3. Spectra resulting from the exact integration of the 3D Schrödinger equation using the laser pulse described in Eq. (1) with $\phi = 0$ (Fig. 1(b)), for different values of the field intensity: threshold of saturation ($I = 3.5 \times 10^{14}$ W/cm^2, light grey line), saturation ($I = 5.6 \times 10^{15}$ W/cm^2, blue line) and deep saturation ($I = 4.2 \times 10^{16}$ W/cm^2, red line). Inset: full spectrum for the deep saturation case, the arrow points the cut-off frequency $I_p + 0.5U_p$, associated to NAT trajectories.

According to our interpretation, the increase of the yields at ultrahigh intensities is a consequence of the non-adiabatic character of the pulse turn-on. Therefore one should expect that pulses with different shapes and lengths but with similar turn-on will give very similar results, as the full ionization of the ground state is achieved practically during the first stage of the interaction. To confirm this point, we have performed exact 3D TDSE calculations of a pulse with the same turn-on as in Eq. (1), followed by two cycles of constant amplitude. For intensities in the deep saturation regime, it is found that the spectrum generated with the longer pulse overlaps the corresponding spectrum for the short pulse (Fig. 3), therefore, confirming that actual shape of the pulse is irrelevant, as long as the turn on coincides.

Finally, the inspection of the 3D TDSE results of Fig. 3 reveals some relevant features for the deep saturation cases. First, the extension is no longer given by the cut-off law, reflecting that the most efficient contributions correspond to trajectories different from the SC type. Although there is no clear cut-off, the extension of the plateau can be well parametrized by the maximum rescattering energy of the NAT-type trajectories, $\simeq I_p + 0.5U_p$. A second characteristic is the absence of structure in the harmonic spectra above the saturation threshold. This is connected to the fact that for a given energy there is a single NAT trajectory, and therefore a single rescattering event generates the high-frequency radiation. This implies the generation of narrow isolated attosecond pulses as already pointed out in [16–19].

In Fig. 4 we show the isolated attosecond pulse generated by the spectrum corresponding to the deep saturation case ($I = 4.2 \times 10^{16}$ W/cm^2) of Fig. 3. The attosecond pulse is obtained filtering the harmonics below *31st*, which corresponds to a photon energy of 46 *eV* (generated by a 800 nm fundamental field) in the spectrum of Fig. 3. Under these conditions a clean, narrow (FWHM$\simeq$ 50 attosecond) and intense attosecond pulse could be synthesized as it is shown in Fig. 4.

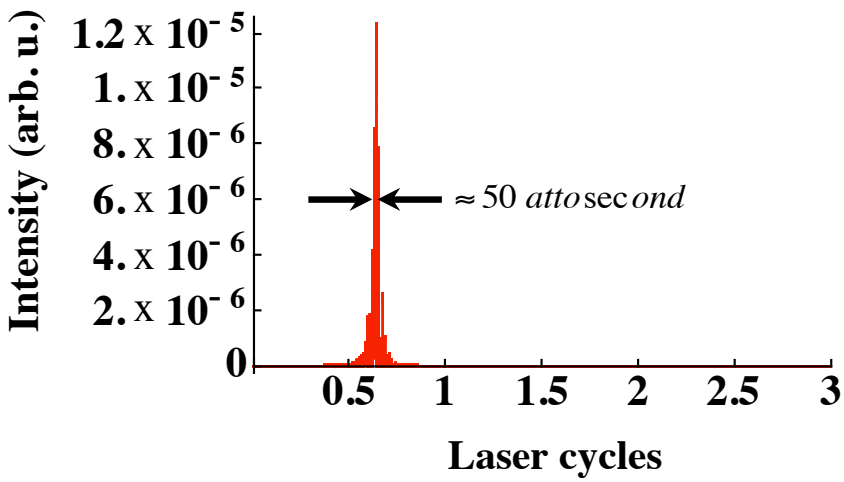

Fig. 4. Isolated attosecond pulse generated from the harmonic spectrum for the case of deep saturation regime ($I = 4.2 \times 10^{16}$ W/cm^2) corresponding to the spectrum in red of Fig. 3. The attosecond is synthesized filtering the harmonics below *31st* (46 eV photon energy).

Due to its non-adiabatic nature, the interaction of NAT pulses with matter is strongly dependent on carrier-envelope phase (CEP), ϕ in Eq. (1). It is not surprising, therefore, that the above scenario changes for CEP different than 0. Fig. 1(c) shows the energy diagram for the trajectories corresponding to the laser pulse of Fig. 1(b), but with $\phi = \pi/2$. In this case, the only relevant trajectories for harmonic generation are of the SC type. NAT trajectories are not useful, as the electron excursion is too short to acquire energy relevant for HHG. As a result, our 3D TDSE calculations for this case show an irreversible decay in yield when the field is increased above saturation.

2.3. Wavelet Analysis

As a final test, in order to confirm more exhaustively our results, we have performed a wavelet analysis (time-frequency analysis) of our 3D TDSE results corresponding to the field parameters in Fig. 1(b).

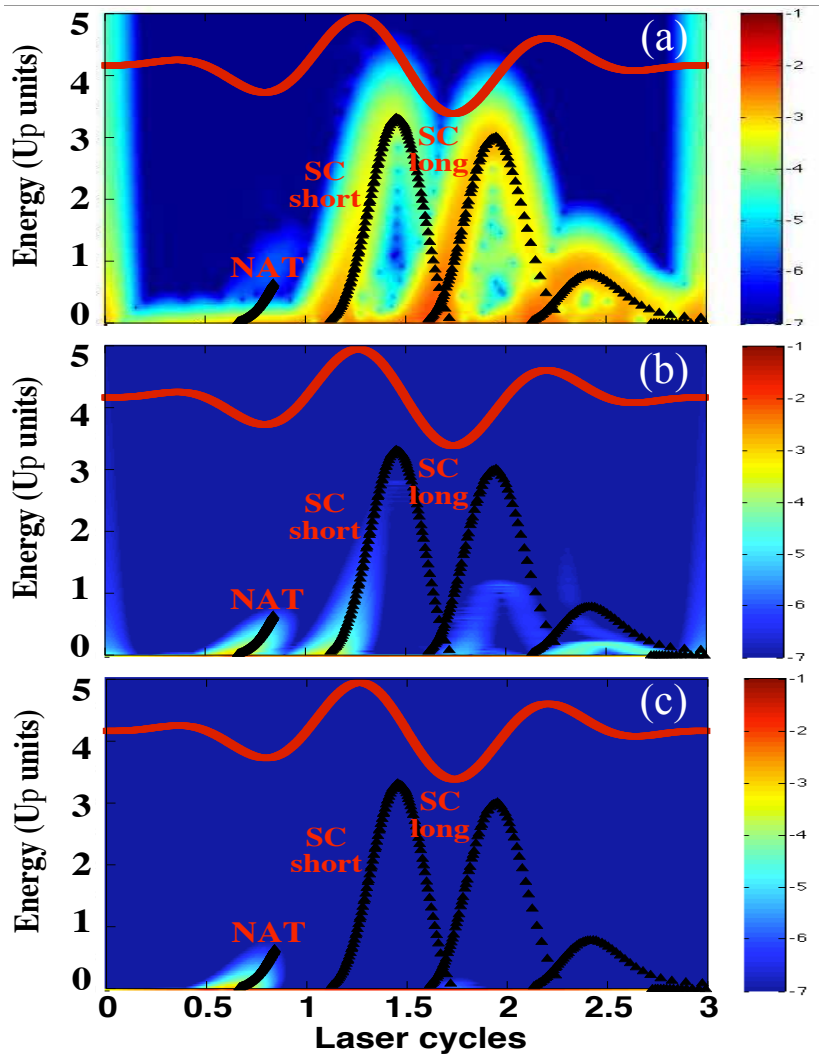

Fig. 5. Wavelet analysis extracted from the exact integration of 3D TDSE, and (superimposed) classical rescattering energies of electrons as a function of the recombination time (black triangles) for laser pulse described in Eq. (1) with $\phi = 0$ and the intensities used in Fig. 3 (in (a) $E_0 = 0.1$ *a.u.*, in (b) $E_0 = 0.4$ *a.u.* and in (c) $E_0 = 1.1$ *a.u.*). The driving laser field is shown in solid red lines. Note that the efficiencies are plotted in the colour bars in an absolute scale (no rescaling is done from one case to the other).

The wavelet analysis is frequently used to extract the information of the particular times and efficiencies at which a certain wavelength is radiated from the results of the exact 3D TDSE. In Fig. 5 we show the wavelet analysis and, superimposed, the resulting rescattering energies computed from the classical trajectories for the three cases reported in Fig. 3. Note that, as the wavelet analysis shows, in Fig. 5(a) harmonics are generated by the usual mechanism (SC short and long trajectories). When the intensity is increasing (Fig. 5(b)) the efficiency of short and long SC trajectories is degraded and NAT trajectories become important. Figure 5(c) shows that at higher intensity regime, only NAT trajectories survive, radiating energies which are in good

agreement with the classical trajectories.

3. Conclusion

In conclusion, we have demonstrated the efficient generation of ultrahigh frequency radiation using pulses with non-adiabatic turn-on with peak intensities in the deep saturation regime. In this case, the harmonic generation is dominated by the contributions of trajectories different than those relevant in the regime below saturation. This new set of trajectories is shown to be resistant to the degradation of the harmonic yield at intensities well above saturation, producing high-order harmonic generation at subnanometer wavelengths. Non-adiabatic turn on pulses emerge, therefore, as a possibility for employing ultra-high intensity near infrared lasers to generate XUV radiation at the water window and beyond. Our results emphasize the interest of developing techniques to obtain CEP controlled ultraintense pulses with non-adiabatic turn-on, without any other constraints regarding the global pulse shape and length.

Acknowledgments

Authors acknowledge support from Spanish Ministerio de Ciencia e Innovación through the Consolider Program SAUUL (CSD2007-00013) and research project FIS2009-09522, from Junta de Castilla y León through the Program for Groups of Excellence (GR27) and from the EC's Seventh Framework Programme (LASERLAB-EUROPE, grant agreement n 228334).

212.128.135.19 (ts '2021-05-19 06:57:45)